Outer Hair Cell Function is Normal in βV Spectrin Knockout Mice.

Michael C. Stankewich[1*], Jun-Ping Bai[2*], Paul R. Stabach[1], Saaim Khan[3], Winston J.T. Tan[6], Alexei Surguchev[6], Lei Song[4], Jon S. Morrow[1,5], Joseph Santos-Sacchi[6,7,8], Dhasakumar S. Navaratnam[2,6,7 ^]

1 Department of Pathology, Yale School of Medicine, New Haven, CT, U.S.A

2 Department of Neurology, Yale School of Medicine, New Haven, CT, U.S.A

3 Cranbrook Kingswood Upper School, MI, USA

4 Department of Otolaryngology-Head and Neck Surgery, Shanghai Ninth People's Hospital, Shanghai Jiaotong University School of Medicine, Shanghai, China

5 Department of Molecular, Cellular, and Developmental Biology, Yale University, New Haven, CT, U.S.A

6 Department of Surgery, Yale School of Medicine, New Haven, CT, U.S.A

7 Department of Neuroscience, Yale School of Medicine, New Haven, CT, U.S.A

8 Department of Cellular and Molecular Physiology, Yale University, New Haven, CT, U.S.A

* Co-first authors
^ Corresponding Author

Address correspondence to Dr. Dhasakumar Navaratnam
Yale School of Medicine, Department of Neurology, PO Box 208018,
New Haven, CT., 06519
email: dhasakumar.navaratnam@yale.edu

Keywords: cochlea, auditory brainstem response, electromotility, distortion product otoacoustic emissions, Spnb5, ribbon synapse, cochlear nerve

ABSTRACT

Reports have proposed a putative role for βV spectrin in outer hair cells (OHCs) of the cochlea. In an ongoing investigation of the role of the cytoskeleton in electromotility, we tested mice with a targeted exon deletion of βV spectrin (Spnb5), and unexpectedly find that Spnb5$^{(-/-)}$ animals' auditory thresholds are unaffected. Similarly, these mice have normal OHC electromechanical activity (otoacoustic emissions) and non-linear capacitance. In contrast, magnitudes of auditory brainstem response (ABR) wave 1-amplitudes are significantly reduced. Evidence of a synaptopathy was absent with normal hair cell CtBP2 counts. In Spnb5$^{(-/-)}$ mice, the number of afferent and efferent nerve fibers is decreased. Consistent with this data, Spnb5 mRNA is present in Type I and II spiral ganglion neurons, but undetectable in OHCs. Together, these data establish that βV spectrin is important for hearing, affecting neuronal structure and function. Significantly, these data exclude βV spectrin as functionally important to OHCs as has been previously suggested.

INTRODUCTION

In the early 1990s, several groups made key seminal observations of a spectrin/actin lattice in the cochlear outer hair cells (OHCs) (Holley & Ashmore, 1990) (Holley, Kalinec, & Kachar, 1992). Their electron micrographs propelled an exquisite model of the spectrin/actin lattice assembled just beneath the OHC lateral membrane with longitudinal spectrin molecules linked to circumferential actin filaments that, in turn, were linked to the plasma membrane by electron-dense pillars. Their work also identified a pool of spectrin in the actin-rich cuticular plate. Another study evaluated spectrin proteins in cochlear innervation during rodent development (Hafidi, Despres, & Romand, 1990). They identified differences in developmental expression of the erythroid beta spectrin (Spnb1 spectrin) compared to the most ubiquitous nonerythroid form αII/ βII spectrin, similar to what is observed in the brain. What is not certain from these earlier studies is the specific spectrins involved, a family now known to consist of two alpha spectrins (Spna1 and 2) and five beta spectrins (Spnb1-5). More recently, it has been shown that Spnb4 is restricted to the nodes of Ranvier in myelinated axons and is also a deafness-related gene (Parkinson et al., 2001) (Lewis et al., 2018). It appears from these studies that the deafness in the quivering mouse is likely not originating in the cochlea but rather is central in origin. Furthermore, Spnb2 spectrin, when selectively deleted from the mouse cochlea sensory epithelia by crossing Spnb2 floxed mice with Atoh-1 Cre-recombinase, causes profound deafness due to disruption of the stereocilia rootlets in the cuticular plate in hair cells (Liu et al., 2019). Thus, the function of specific spectrins, particularly

78 as it relates to the OHC lateral membrane and cochlear innervation, remains
79 unclear. In humans, the molecule βV spectrin (SPTBN5) that was first discovered
80 in the retina, is involved with the retinal disorder, Usher syndrome (Stabach &
81 Morrow, 2000) (Papal et al., 2013). Further reports have proposed a putative role
82 for βV spectrin in a second sensorineural function, hearing. One group's
83 observations demonstrated that antisera raised against the C-terminal peptide of
84 SPTBN5, labeled structures along the lateral membrane of the OHC (Legendre,
85 Safieddine, Kussel-Andermann, Petit, & El-Amraoui, 2008) (Cortese et al., 2017).
86 This observation drew attention because detection of this giant spectrin in tissue
87 other than retina and testis has been elusive. This finding raised the possibility that
88 βV spectrin was involved in the electromotile response of OHCs.

89 Continuing an ongoing effort in our lab to define the cytoskeleton's role in
90 electromotility (Bai et al., 2010), we sought to determine the role of βV spectrin in
91 OHC function. In this study, we analyzed βV spectrin expression in the cochlea
92 and addressed its function in mice with a targeted deletion of Spnb5. We tested
93 hearing by auditory brainstem responses (ABRs), measured OHC-mediated
94 otoacoustic emissions and OHC nonlinear capacitance (NLC), and evaluated the
95 number of inner hair cell (IHC) ribbon synapses and nerve fibers that innervate the
96 cochlear sensory epithelium. We find that while OHC function is unaffected in the
97 absence of βV spectrin, nerve counts are reduced at the habenular, in all three
98 turns of the cochlea, and in efferent fibers in the mid and basal turns, which
99 collectively account for the reduced wave I amplitudes in ABRs. Using RNAscope
100 *in situ* hybridization, we confirm expression of Spnb5 mRNA in Type I and II SGNs

101 and absent expression in OHCs. Moreover, mRNA transcript was significantly
102 reduced in the SGN of Spnb5$^{(-/-)}$ mice, confirming knockdown of the gene. We
103 conclude that βV spectrin is necessary to maintain the integrity or function of
104 afferent and efferent nerves of the peripheral auditory system, but plays no role in
105 the OHC itself.
106
107

RESULTS

Mouse βV spectrin amino acid sequence is divergent from the human protein.

Surprisingly, a sequence alignment comparing the mouse amino acid sequence to the human amino acid sequence reveals a significant divergence. In contrast, other beta spectrins, including beta I-IV, have ~ 90% amino acid conservation between human and mouse sequences. By aligning human and mouse βV spectrin, we note a significant divergence at the N- and C-termini of the proteins and an internal stretch of amino acids from position 817-922 (**Figure 1A**). Of note is that the initiator methionine residue in the human form is conserved between mouse and human genes and lies at position 36 and within exon 2 (**Figure 2**). The mouse sequence incorporates an unusual homorepeat of glutamines and, notably, does not have a bona fide pleckstrin homology (PH) domain seen in the human form.

Spnb5 mRNA tissue expression.

Spnb5 spectrin is expressed in most mouse tissues but at low levels. In ENCODE, the level of Spnb5 transcripts is an order of magnitude less abundant than the ubiquitous form Spnb2 (**Figure 1B**) (Yue et al., 2014). The peak abundance of Spnb2 approaches 50 RPKM while Spnb5 is 0.5 RPKM in testis (**Figure 1B, C**). Interestingly, the GTEX dataset shows high expression of Spnb5 in the peripheral (tibial) nerve (**Figure 1D**). To validate that mRNA is detected in mice, we tested RNA from the testis with primer sets that bridged exons. By standard RT-PCR, Spnb5 mRNA fragments encoding both the N-terminus and C-terminus were

132 amplified from testis and brain RNA, and its identity was confirmed by Sanger
133 sequencing. In contrast to brain and testicular tissue, we could not detect Spnb5
134 mRNA in isolated OHCs and whole organ of Corti by both conventional and nested
135 PCR (Table 1 details the gene-specific primer sets). Using RT-PCR from ~3000
136 OHCs and organ of Corti, we detect both Spnb1 and Spnb2. Using nested PCR,
137 amplicons for these spectrins are robust, while we do not visualize any product for
138 Spnb5 (**Figure 1E**). These data are in accord with data derived from the public
139 data sets of transcriptome profiling for OHCs in gEAR (https://umgear.org/) (**See**
140 **supplementary Figure1**)**.** Furthermore, *in situ* hybridization for Spnb5 using
141 RNAscope corroborates these findings. We are unable to detect Spnb5 mRNA in
142 OHCs (**see Supplementary Figure 2, panels C and S)**, whereas mRNA for the
143 potassium channel, Kcnma1, is readily detected in OHCs (green signal in **panel**
144 **B)**. In contrast, the Spnb5 probe is detected in spiral ganglion neurons (SGNs) (red
145 signal in both **panels C and P)**. To further characterize the expression of Spnb5
146 in SGNs, we co-labeled Spnb5 (green) with known markers of myelinated Type I
147 ganglion cells (tyrosine hydroxylase, (TH)) and unmyelinated Type II ganglion cells
148 (Epha4) in red (see Supplementary Figure 3). We find that Spnb5 signal overlaps
149 with the signals from both TH (panel A) and Epha4 (panel B). These data
150 demonstrate that Spnb5 is expressed in both Type I and II SGNs.
151

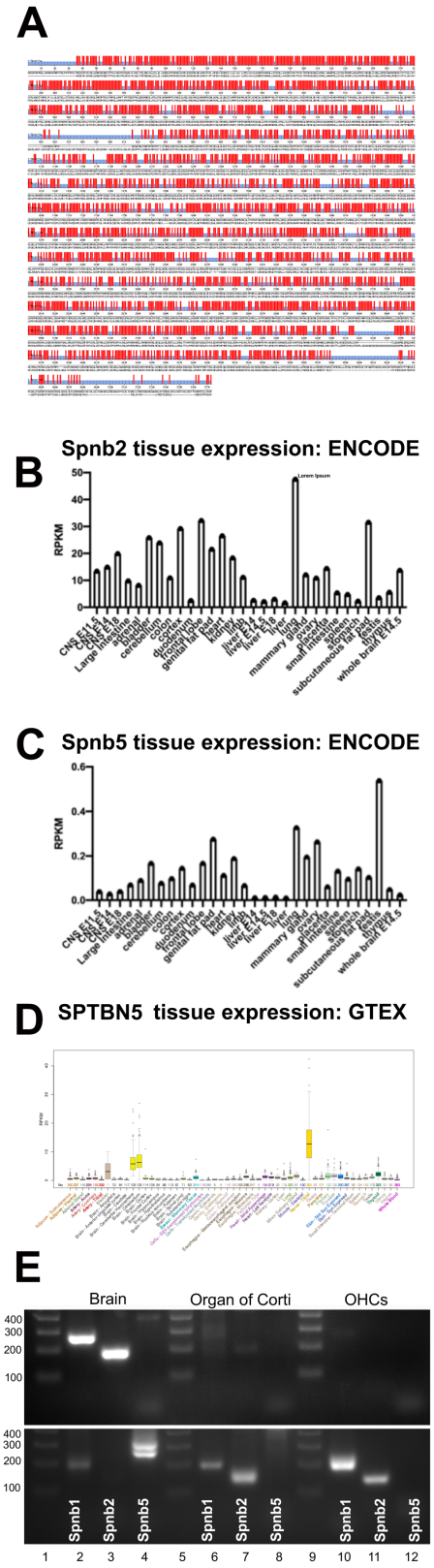

Figure 1. (A) Spnb5 mouse (ENSMUST00000156159.4) **amino acid sequence differs from humans.** Shown is the comparison of the deduced amino acid sequence of mouse (lower) and human (upper) Spnb5. Conserved amino acids are marked in red. There is divergence at the N and C termini. In addition, a region in the middle of the protein from posiiton 817-922 shows significant divergence. The mouse version of this gene shares only 65.6 percent identity with the human form. **(B, C) Spnb5 is expressed in brain and testis.** The relative abundance of Spnb2 transcripts as compared to Spnb5 in mouse tissues. Shown are the expression of Spnb2 and 5 in RNA Seq. NCBI reference datasets (ENCODE; Bioproject PRJNA66167_(Yue et al., 2014). On average, the abundance of Spnb5 mRNA is an order of magnitude less abundant than Spnb2. Of the tissues examined, adult testis has the most mRNA for Spnb5. **(D) In human, Spnb5 is most expressed in peripheral nerve.** The relative abundence of Spnb5 in different tissues in GTEX database is presented (version 6) (Consortium, 2013). Of all the tissues examined Spnb5 is expressed in highest amounts in the peripheral nerve (tibial nerve). **(E) Spnb5 mRNA is not detectable in the organ of Corti or OHCs.** Shown are PCR amplifications from mouse brain (lanes 2-4), organ of Corti (lanes 6-8) and OHCs (lanes 10-12) of Spnb1 (lanes 2, 6 and 10), Spnb2 (lanes 3, 7 and 11) and Spnb5 (lanes 4, 8 and 12). The upper panel shows amplicons for these three mRNA transcripts using outer primers while the lower panel shows amplicons of primers using a nested set of primers. All three spectrins are detectable in brain. Spnb1 and 2 are detectable in both the organ of Corti and OHCs (lanes 6-7 and 10-11). Spnb5 however, is not detectable using

Figure 1

154 **Supplementary Figure 1.**

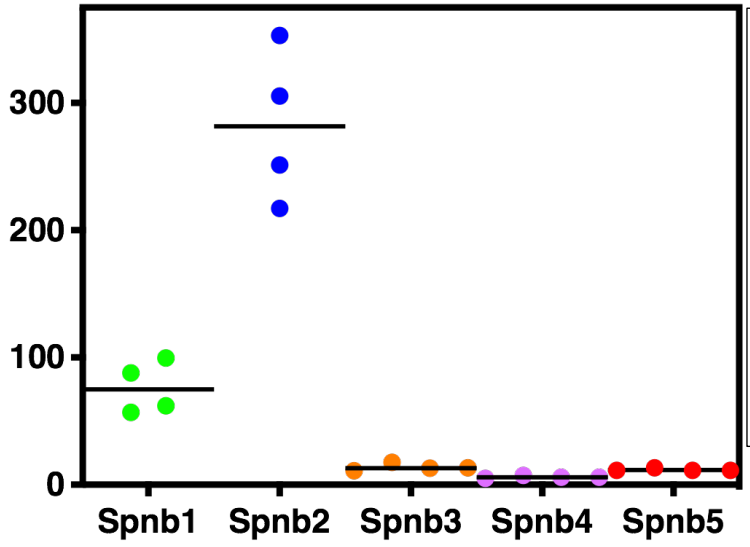

Figure S1. Expression levels for each of the beta spectrins in OHCs. Mining data from the gene Expression Analysis Resource (gEAR) we graphed the abundance of each of the five beta spectrin genes. This data set was derived from transcriptome analysis using sc-RNAseq of cell populations isolated from mouse cochleae (Li et al., 2018).

155
156
157

158 **Targeted knockout of Spnb5 in mice using homologous recombination.**

159 In order to properly target the βV spectrin gene in mice, we needed to know its
160 precise gene structure. While the human gene has been well characterized and
161 indexed since its discovery in 2000 (Stabach & Morrow, 2000), there has been
162 ambiguity in the intron/exon usage in the mouse gene found on chromosome 2.
163 The GENBANK entry for Spnb5 has been modified many times in the last several
164 years, with the last significant annotation in 2007 (Benson et al., 2013). This
165 annotation was derived by automated computational analysis using gene
166 prediction algorithms. The exon prediction is made difficult because 1) the gene is
167 very large, so PCR amplifying a full-length cDNA is not trivial, and 2) the
168 conservation between human and mouse intron/exon boundaries is weak at the N-
169 and C-termini. The current and accepted annotated version in both the UCSC
170 genome browser and in Ensembl shows Spnb5 spectrin mRNA in the mouse to be
171 14.4 kb with a 10,872 bp ORF that has 66 exons and codes for 3623 amino acids:

172 NM_001370938: NP_001357867.1. This version has been validated in the
173 ENCODE project based on the robustness of next-generation sequencing efforts
174 over the last several years (Yue et al., 2014).
175
176 Shown in the schematic in Figure 2A is the strategy for targeted deletion of exon
177 2 of Spnb5. The knockout strategy was based on the transcript ID:
178 ENSMUST00000156159.3, and a targeting construct was generated in which
179 three Lox P sites were inserted to flank the neomycin selection marker and exon
180 2 containing the start codon, resulting in disruption of the open reading frame upon
181 Cre-mediated excision. Exon 2 contains the ATG start codon (with a consensus
182 Kozak sequence) and an additional 37 amino acids at its N-terminus. Notably, the
183 codon for the methionine residue corresponding to the human start codon is also
184 contained within the second exon. A genomic bacterial artificial chromosome
185 containing the Spnb5 locus was obtained, and genomic DNA fragments containing
186 the first exons of Spnb5 were subcloned in pEasy (a gift from Sankar Ghosh). The
187 targeting vector comprised a 4.3 kb long arm, a 4.1 kb short arm, and a middle
188 selection cassette which contains exon two flanked by a PGK–neomycin
189 resistance (Neo), two FRT sites, and the herpes simplex thymidine kinase gene
190 (Figure 2B and Primer Sets in Table 2). The targeting plasmid DNA was linearized
191 with Cla1 and electroporated into mouse embryonic stem cells (ESCs)
192 (129SV/EV). ESCs were selected for neomycin/G418 resistance. Positive clones
193 were identified by PCR and confirmed by Southern blot analysis using external
194 and internal probes. A correctly targeted ESC clone was injected into C57BL/6J

195 blastocysts to produce germline transmitting chimeric mice. These were then
196 mated with actin-Cre C57BL/6J transgenic mice for generation of heterozygous
197 Spnb5 transgenic mice with both the Neo cassette and exon two removed
198 (Spnb5$^{(+/-)}$). The resulting Spnb5$^{(+/-)}$ offspring were crossed to generate βV
199 spectrin-deficient mice. The genotypes of these mice were confirmed by PCR
200 amplification (Figure 2C). Chimeric mice were backcrossed onto the C57BL/6J
201 strain. Litters from heterozygous breeders Spnb5$^{(+/-)}$ / Spnb5$^{(+/-)}$ were of normal
202 number, and the mice of all genotypes were phenotypically indistinguishable with
203 normal lifespans >2 yrs. old. We confirmed decreased expression of Spnb5 in
204 cDNA from testes of Spnb5$^{(-/-)}$ mice, where we found equivalent expression of
205 Spnb2 and Spna2 (Figure 2D and Primer Sets in Table 3). The decreased level of
206 Spnb5 mRNA was corroborated by RNAScope in situ hybridization (ISH)
207 experiments. In low power images of cochlear tissue (Supplementary Figure 2,
208 panels A- I), the signal for Spnb5 (red) in the SGN is significantly reduced in KO
209 mice. Quantitation of the mean fluorescence intensity shown in panel V reveals
210 that the amount of signal in SGNs is significantly reduced by greater than 60% in
211 the SGN of Spnb5$^{(-/-)}$ animals. Higher power magnification ISH images, when
212 labeled with Spnb5 probe alone, reveals a significant reduction in both the number
213 of fluorescent particles per neuron in KO tissue (panel W). On average, the number
214 of particles per neuron with positive granules was significantly reduced by greater
215 than ~50%. In addition, both the total fluorescence intensity and the number of
216 neurons that contained Spnb5 is dramatically reduced in the SGNs of Spnb5$^{(-/-)}$
217 animals (panel C vs. F). The binding site for the RNAscope *in situ* probes (at

218 position 7163 – 8000 in XM_006500537; 3669-4506 in ENSMUST00000156159.4)
219 corresponds to ~ 1300 amino acids after the initiator methionine. These data
220 suggest that the transcript up to position 3669-4506 was significantly reduced in
221 the SGN of knockout animals. It should be noted that the actin binding of spectrins
222 occurs through calponin homology (CH1 and CH2) sites present at the N-terminus
223 of the proteins. In Spnb5, these sites are located at aa 20-124 (CH1) and aa 143-
224 247 (CH2) and encoded by the transcript well before the RNAscope *in situ* probe
225 binding sites. In other beta spectrins, loss of function mutations occur within the
226 CH1 and CH2 actin binding domains (Cousin et al., 2020). While it is still possible
227 that there are mRNA transcripts that are shorter with in-frame methionine start
228 sites, these transcripts would not be expected to produce a functional protein in
229 lieu of it lacking the CH1 and CH2 actin binding domains (there are, for instance,
230 43 in-frame methionine codons, 19 of which also contain consensus Kozak
231 sequences, that lie downstream of the *in situ* hybridization probe binding sites).
232
233

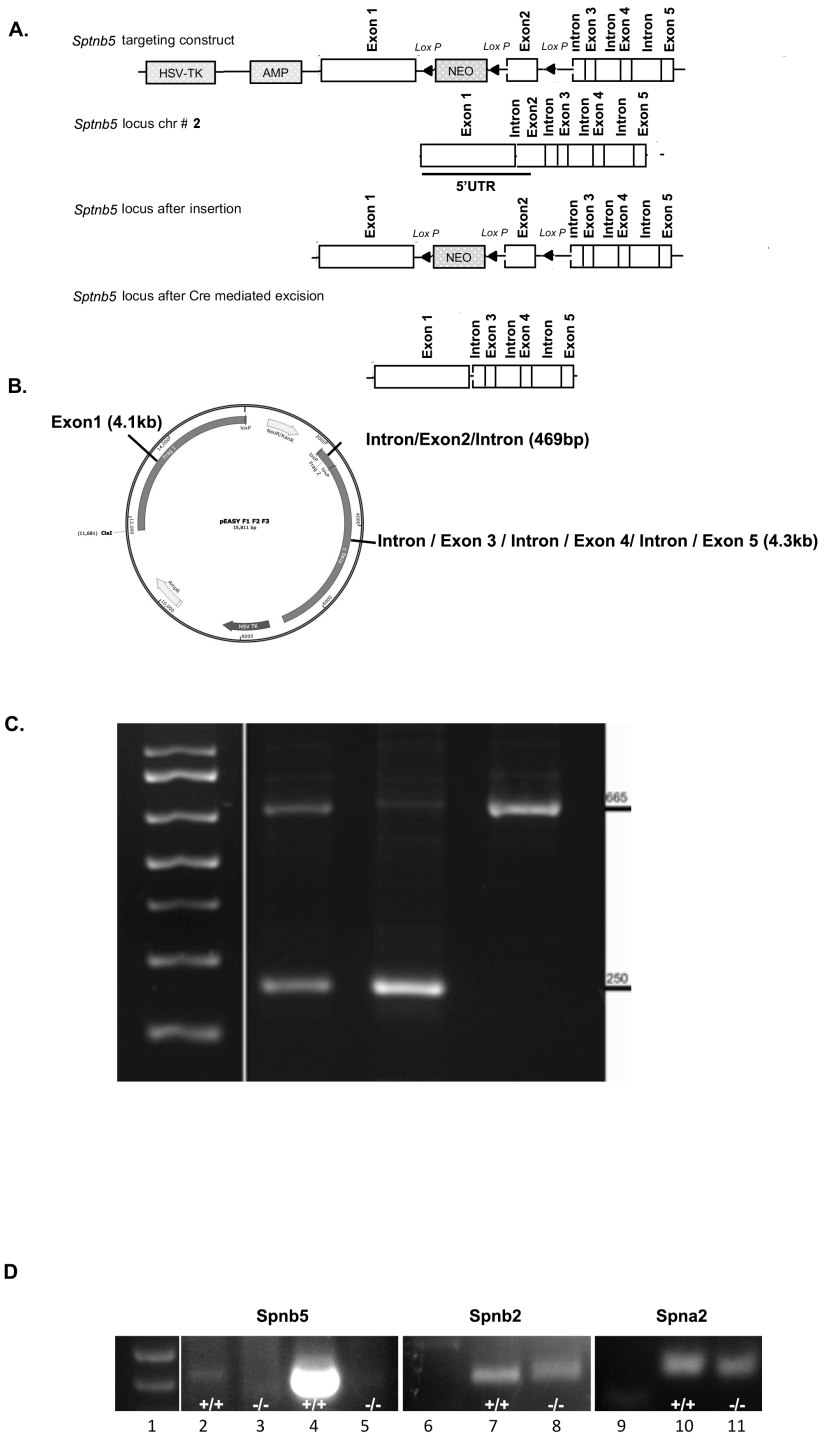

Figure 2. Exon 2 of the Spnb5 gene was removed using homologous recombination. (A) Schematic of the strategy used to delete exon 2. The construct contained a short arm of exon 1 and a long arm of exons 3, 4, and 5 together with the intervening introns. Both the selection marker Neo and exon two are flanked by Lox P sites. Linearized plasmid was injected into ES cells and clones with homologous recombination and selected by neomycin (Neo)/ G418 resistance. Mice were then crossed with Actin-Cre mice to generate floxed mice lacking the Neo cassette and exon 2. **(B) Vector map of pEASY used to target Spnb5 deletion.** Exon 2 was subcloned between two Lox P sites adjacent to the Neo gene. These two genomic fragments were in turn placed between a 4.1kb short arm containing Exon 1 and a 4.3kb long arm containing exons 3, 4, and 5 and the intervening introns. The vector also contains a thymidine kinase and ampicillin gene allowing for selection. The plasmid was linearized with Cla1. **(C) PCR amplification of genomic DNA confirming deletion of exon two and flanking intronic sequence.** In genomic DNA from Spnb5$^{(-/-)}$ mice**,** primers that amplify a product no longer contain part of intron 1; exon 2; and part of intron 2/3. Lane 1 base pair standards, lane 2 Spnb5$^{(+/-)}$, lane 3 Spnb5$^{(-/-)}$, lane 4 Spnb5$^{(+/+)}$. The larger fragment of 665 bp consists of unexcised exon two while the smaller fragment consists of genomic DNA fragment from which exon two has been excised. **(D) Decreased expression of Spnb5 in Spnb5$^{(-/-)}$ testicular cDNA compared to Spnb2 and Spna2**. Spnb5 exons 58-60 in lanes 2-3, Spnb5 exon 53-55 in lanes 4-5; Spnb2 in lanes 7-8 (exons 28-29) and Spna2 (exons 54-55) in lanes 10-11**.** WT in lanes 2, 4, 7 and 10. Spnb5$^{(-/-)}$ in lanes 3, 5, 8 and 11.

Figure 2

234
235
236

237 **Supplementary Figure 2.**

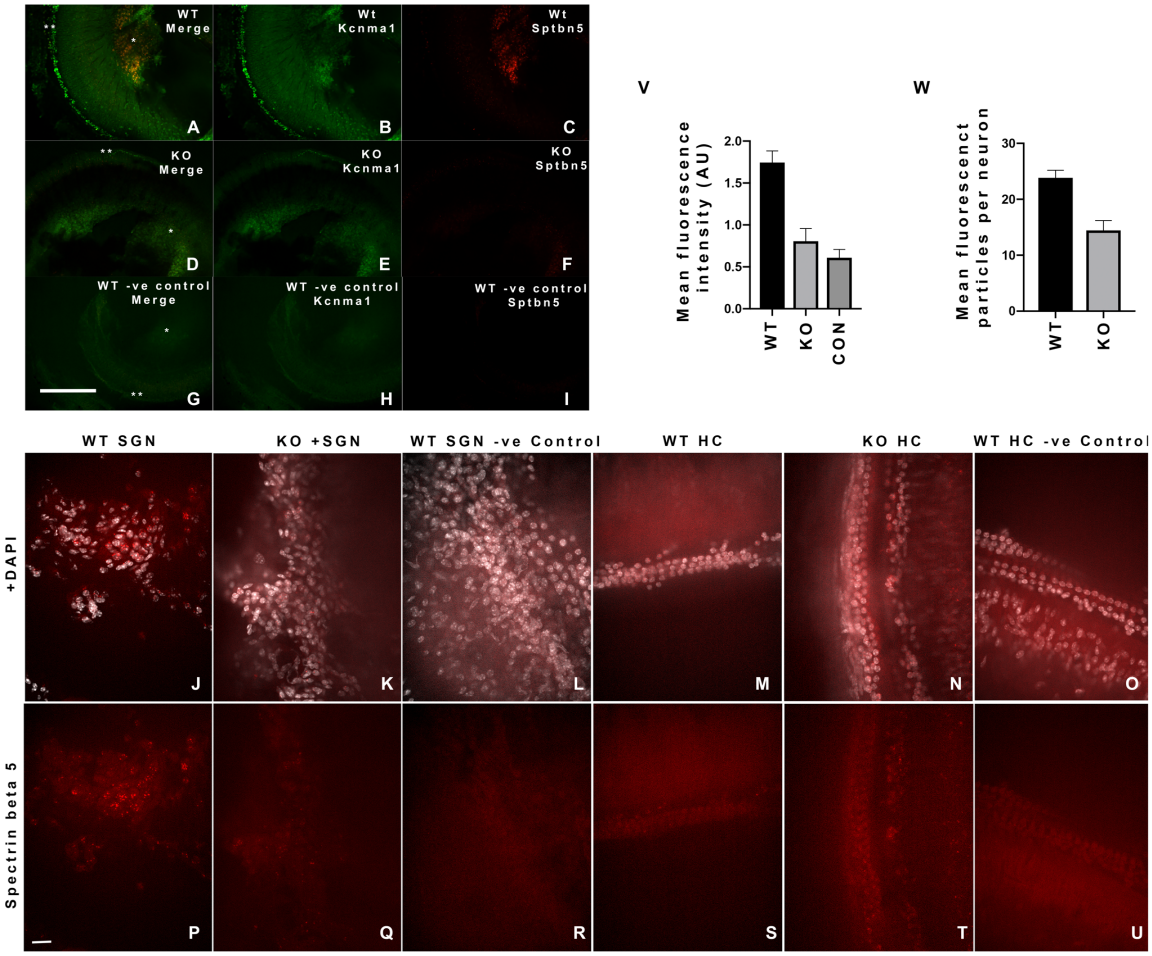

238
239
240 **Figure S2. *In situ* hybridization (RNAscope) shows the expression of Spnb5 and**
241 **Kcnma1 in WT and Spnb5$^{(-/-)}$ cochlear tissue**. In the top image, panels (A-F) are a low
242 magnification (10x) comparison of Spnb5 mRNA (red, C & F) and Kcnma1 mRNA (green,
243 B & E) between WT and KO from the apical turn of the organ of Corti. Merged images are
244 displayed in panels (A & D) and the DapB negative control images (-ve control) are shown
245 in panels (G-I). Single asterisks indicate spiral ganglion neurons (SGNs) and double
246 asterisks highlight regions with hair cells (HC). Mean SGN Spnb5 fluorescence intensity
247 of WT animals were significantly different from KO animals and negative controls (V) (WT
248 1.744 ± 0.13 SEM, n = 9, KO 0.80 ± 0.15 SEM, n = 7, -ve control 0.60 ± 0.09 SEM, n = 5
249 one-way ANOVA, $p<0.001$). Areas of SGNs were demarcated based on staining of nuclei
250 (DAPI). Scale bar, 200 μm. The bottom image (J-U) is a single-color, high magnification
251 (40x) for WT and KO tissue. mRNA for Spnb5 was assessed in the SGNs (P-R) and HCs
252 (S-U). The upper panels (J-O) are the same images with DAPI demarcating cell nuclei.
253 Panels (J,P,K,Q) representing Spnb5 mRNA levels (red signal) in WT and KO animals
254 show reduced expression of Spnb5 mRNA in KO animals. Negative control (DapB) images
255 are shown in panels L & R. Of note, Spnb5 is not expressed in all SGNs. In KO animals,
256 the number of Spnb5 granules per neuron, the overall fluorescence intensity of these
257 granules, and the number of neurons with granules were all reduced compared to WT
animals. Mean number of Spnb5 mRNA granules per SGN in WT and KO mice (W) were
significantly different (WT 23.8 ± 1.3 SEM, n = 23 and KO 14.4 ± 1.7 SEM, n = 28 neurons,
respectively, students t test, $P <0.001$). Here, only those neurons with Spnb5 signal were
included. Panels (M,S,N,T) of Spnb5 in HCs of WT and KO cochlea show no signal above
DapB background (O & U). Scale bar, 20 μm.

258 **Supplementary Figure 3.**

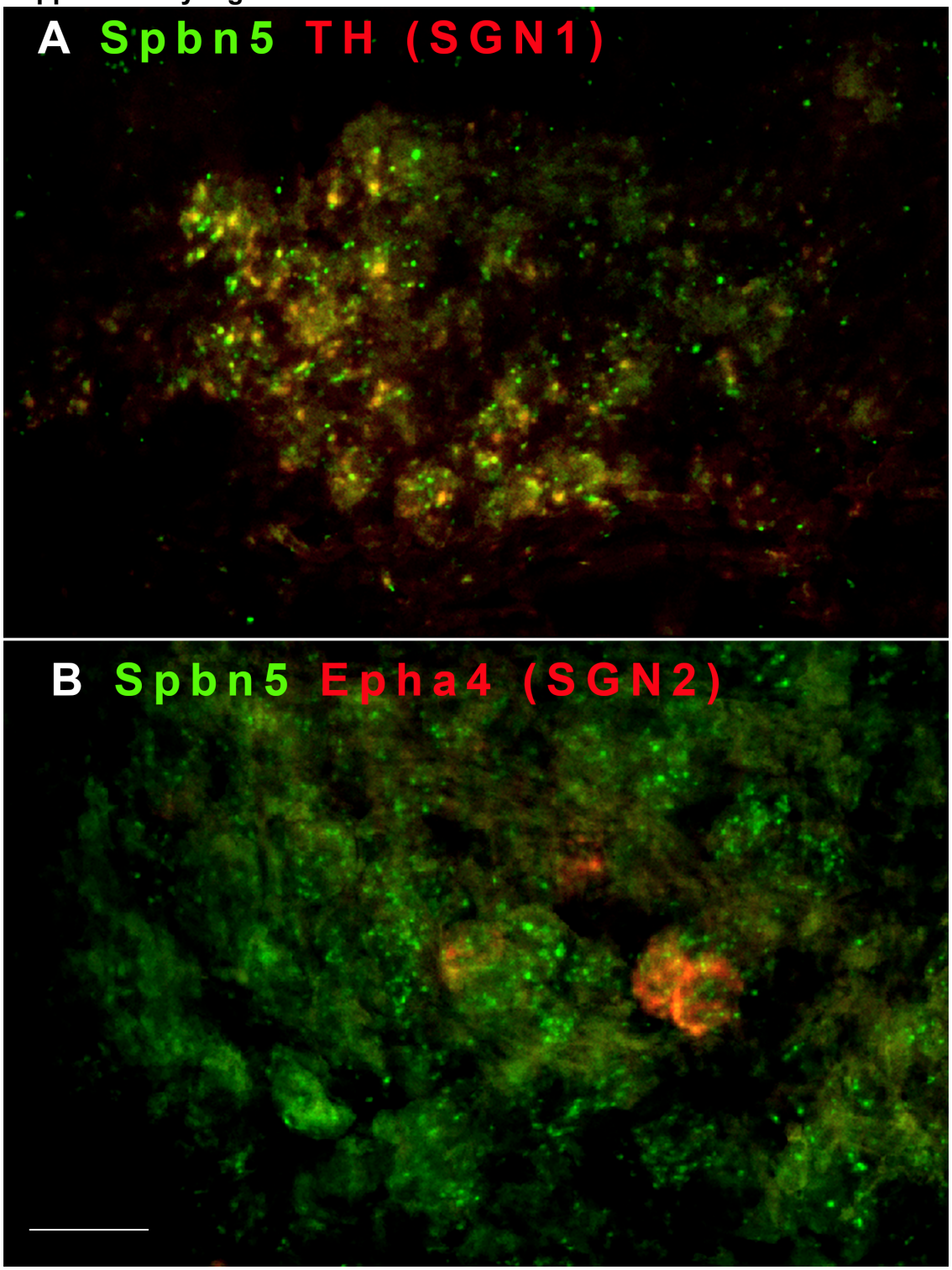

259
260
261
262
263

Figure S3. *In situ* hybridization (RNAscope) shows the expression of Spnb5 in SGNs I and II. In the top image, panel (A) is a merged high magnification (40x) comparison of Spnb5 (green) and tyrosine hydroxylase (TH) (red) mRNA. Yellow granules in this image demarcate coincident RNA labeling in SGN Type I cells. Panel (B) is a merged image of Spnb5 (green) and Epha4 (red) signals. Yellow granules are coincident labeling of Spnb5 and Epha4 mRNA in three SGN Type II cells. Scale bar, 20 μm.

264 **Auditory thresholds and OHC function are similar between Spnb5$^{(-/-)}$ and**
265 **control mice.**
266 To investigate how the loss of Spnb5 impacts auditory information processing, we
267 compared the *in vivo* ABRs of 2-month-old Spnb5$^{(+/+)}$ and Spnb5$^{(-/-)}$ mice. ABR
268 thresholds remained unaltered in Spnb5$^{(-/-)}$ mice across all sound frequencies
269 tested (**Figure 3A**). We also found that distortion product otoacoustic emissions
270 (DPOAEs), a measure of the robustness of OHC function, were unaffected by the
271 loss of Spnb5 (**Figure 3B**). These findings with preserved DPOAE thresholds also
272 extended to suprathreshold responses at sound intensities of 80-90 dB SPL
273 (**Figure 3C**). Since spectrins have been implicated in membrane integrity and
274 protein shuttling, we also assayed prestin expression in the lateral wall using its
275 gating charge movement (NLC) at postnatal day 13 (when prestin expression
276 increases in OHCs) and at two months (Abe et al., 2007). At both these time points,
277 we found NLC to be unaffected in Spnb5$^{(-/-)}$ mice (**Figure 4A**). Our measures of
278 the different parameters of NLC, Q_{sp}, V_h, and z, were similar between WT and
279 Spnb5$^{(-/-)}$ mice (**Figure 4, A-D**).

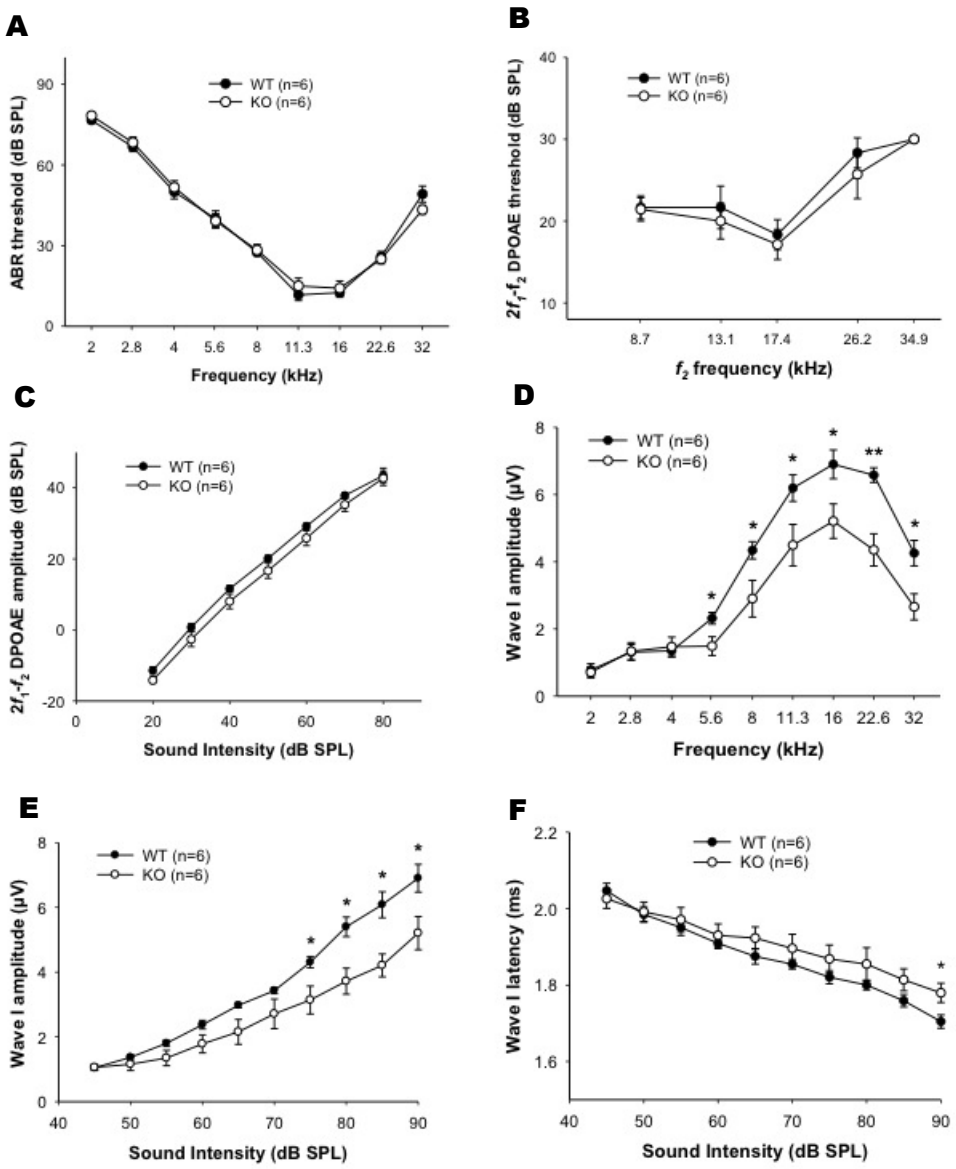

Figure 3

Figure 3. ABR analysis suggests a neuronal and not OHC dysfunction in Spnb5$^{(-/-)}$ mice. (A) ABR thresholds at frequencies between 2-32 kHz remain unchanged in Spnb5$^{(-/-)}$ mice. ABR thresholds in Spnb5$^{(-/-)}$ (open circle) and littermate WT (solid circle) mice at 2 months of age are plotted as a function of stimulus frequency. There are no significant differences between WT and Spnb5$^{(-/-)}$ mice at all frequencies tested from 2 to 32 kHz. **(B) Similar $2f_1$-f_2 DPOAE thresholds are observed in 2-month-old WT and Spnb5$^{(-/-)}$ mice at all f_2 frequencies tested**. **(C) $2f_1$-f_2 DPOAE amplitudes are unaffected in Spnb5$^{(-/-)}$ mice.** Input/output (I/O) function analysis of **$2f_1$-f_2** DPOAE responses in WT (solid circle) and Spnb5$^{(-/-)}$ (open circle) mice as a function of sound intensity at the f_2 frequency of 17.4 kHz at 2 months of age are graphed. DPOAE amplitudes in Spnb5$^{(-/-)}$ mice show no significant differences across all sound intensities compared to WT mice. **(D) ABR wave I amplitudes are significantly altered between Spnb5$^{(-/-)}$ and WT at high stimulus intensities at frequencies between 5.6-32 kHz, but not at frequencies between 2-4 kHz.** Shown are wave I amplitudes at 90 dB SPL. There is a consistent reduction in wave I amplitudes at these suprathreshold intensities from 5.6-32 kHz. **(E) ABR wave I amplitudes at 16 kHz are significantly reduced in Spnb5$^{(-/-)}$ mice at high sound intensities (75-90 dB SPL). (F) ABR wave I latencies at 16 kHz are significantly delayed in Spnb5$^{(-/-)}$ mice at 90 dB SPL.** Latencies at all other frequencies are not significantly delayed (data not shown). Data are means +/- SEM. The number (n) of animals per experiment is shown in each graph. Asterisks indicate $p<0.05$.

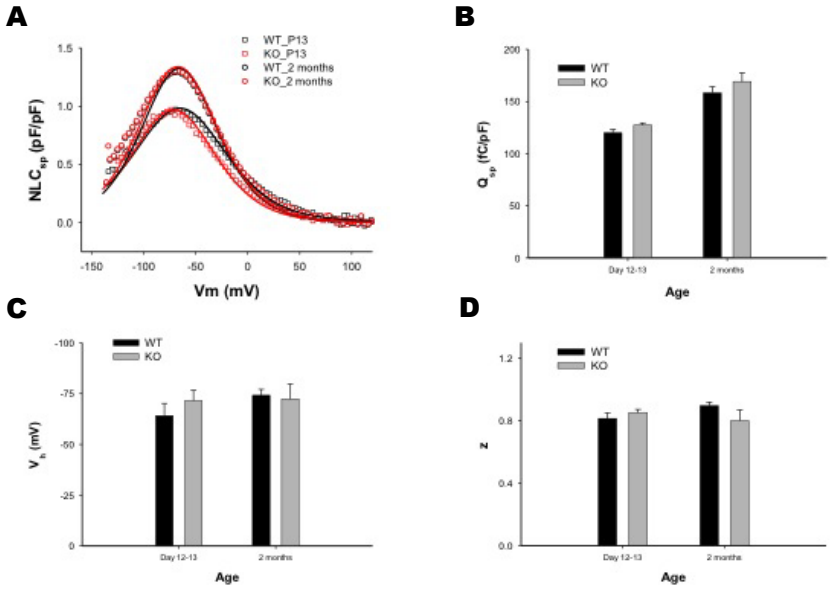

Figure 4

285
286

Figure 4. Spnb5$^{(-/-)}$ mice have similar nonlinear capacitance characteristics as controls at two age groups. NLC was measured at postnatal day 13, a midpoint of NLC development, and at two months when hearing is mature. **(A**) **There are no significant effects of OHC NLC in Spnb5$^{(-/-)}$ mice.** Shown are representative traces of NLC measurement in Spnb5$^{(-/-)}$ and WT mice. There are no differences in NLC between Spnb5$^{(-/-)}$ and WT mice at these two time points. **B, C, and D**. **NLC parameters are unaffected in Spnb5$^{(-/-)}$ mice.** Shown are means (+/- SEM) of NLC parameters in Spnb5$^{(+/+)}$ and Spnb5$^{(-/-)}$ mice at 13 days and two months, with no significant differences (P>0.05) in all of these measures (Q_{sp}, V_h and z). **(B) Q_{sp}, a specific measure of net charge movement per unit of membrane corrected for linear capacitance. (C) V_h, a measure of the voltage dependence of charge movement. (D) z, a measure of the slope in NLC voltage dependence and indicative of the unitary charge movement.**

287 **Loss of βV spectrin affects hearing sensitivity in a manner suggesting a**
288 **neural processing disorder.**
289 The ABR is characterized by a series of electrical waves representing the
290 progressive transfer of the auditory signal from the periphery to the CNS (Song,
291 McGee, & Walsh, 2006). Wave I represents the summated response from the
292 spiral ganglion and auditory nerve (Melcher et al., 1996). While we see no
293 differences in ABR thresholds, we note that wave I amplitudes from 5.6 kHz and
294 upwards are significantly altered between Spnb5$^{(-/-)}$ and WT mice at high stimulus
295 intensities (suprathreshold) (**Figure 3D**). We also analyzed the latency of wave I
296 to investigate any potential changes in the rate of propagation of neural
297 transmission. Wave I latency at 16 kHz was progressively delayed at high sound
298 intensities reaching significance at the highest sound intensity (90 dB SPL) (**Figure**
299 **3F**). Latencies at other frequencies were not significantly different from WT.
300
301 **Spnb5 plays a critical role in sensorineural processing.**
302 What could be the cause of the differences in amplitudes of wave I between WT
303 and Spnb5$^{(-/-)}$ mice? We sought to exclude synaptopathy as a cause of the
304 decrease in wave I amplitudes. For instance, spectrins have been shown to be
305 important in targeting structural elements of the synaptic apparatus as well as
306 maintaining the integrity and compartmentalization of axons and dendrites
307 ((Hammarlund, Jorgensen, & Bastiani, 2007), (Stankewich et al., 2010), (Efimova
308 et al., 2017; Stankewich et al., 2011), (Lorenzo et al., 2019). We compared the
309 number of IHC ribbon synapses in the basal, middle, and apical turn of the organ

310 of Corti between Spnb5$^{(-/-)}$ and WT mice. We used antibody labeling of the marker
311 protein CtBP2 (Bramhall, McMillan, Kujawa, & Konrad-Martin, 2018), a major
312 component of the ribbon synapses, and a well-defined marker of synaptopathy
313 (Sergeyenko, Lall, Liberman, & Kujawa, 2013). We found no differences in CtBP2-
314 labeled synaptic boutons of IHCs in the three cochlear turns between WT and
315 Spnb5$^{(-/-)}$ mice (**Figure 5A**). We then sought to identify morphological differences
316 in afferent nerve numbers as a possible cause of the reduced wave I amplitudes.
317 We found significant reductions in neurofilament labeled, nonmyelinated, afferent
318 fibers in the habenular in all three turns as well as efferent fibers in the basal and
319 middle turns of the cochlea (**Figure 5H, O**).

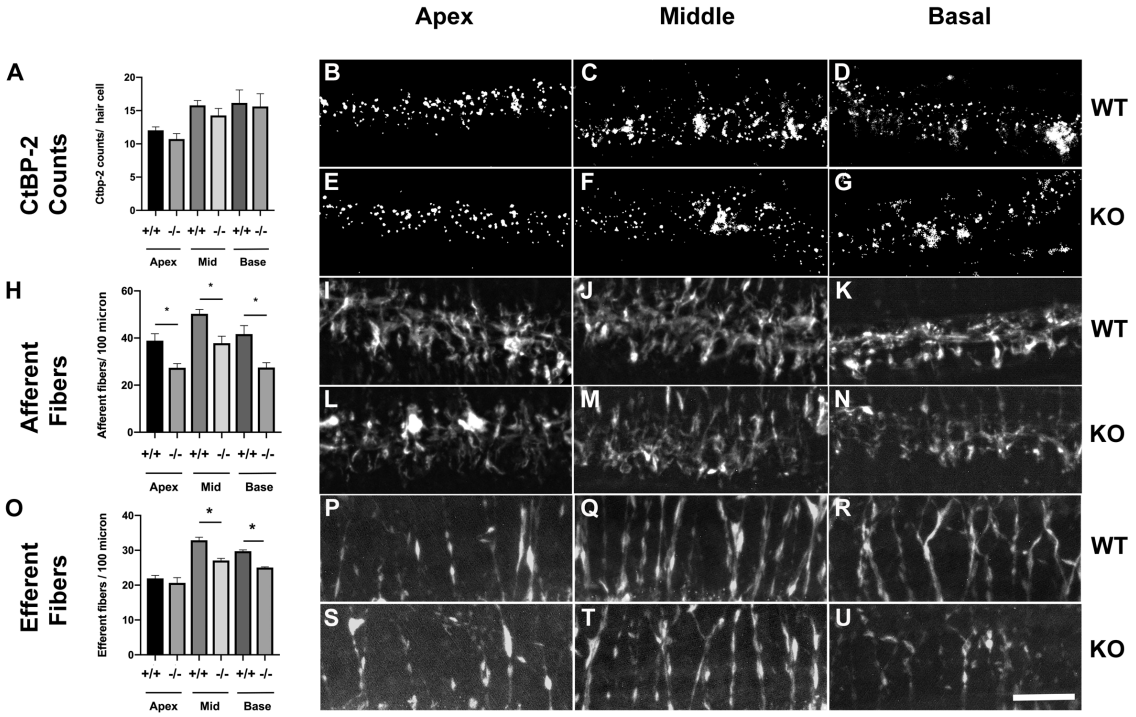

320 **Figure 5**

321

322

323 **Figure 5. Spnb5$^{(-/-)}$ mice show evidence of neuropathy and no evidence of a synaptopathy.** Shown are representative z axis projections of confocal micrographs of WT
324 and βV spectrin KO mice in which synaptic boutons are labeled with antibodies to CtBP2 (**B-G**). **Afferent (I-N) and efferent (P-U) nerve fibers are labeled with antibodies to**
325 **neurofilament.** The scale bar equates to 20 microns. There is a significant reduction in the density of afferent fibers at the habenular in all three turns and efferent fibers in the cochlear
326 canal of Spnb5$^{(-/-)}$ mice. In contrast, there are no differences in CtBP2-positive bouton counts in all three turns of the cochlea. (**A, H, O) Shown are mean (+/- SEM) counts of synapses**
327 **per IHC (A), afferent fibers (H), and efferent fibers (O) in all three cochlear turns.** The differences in afferent and efferent counts are significant (* $P<0.05$, n = 4 cochlea) between
328 WT and Spnb5$^{(-/-)}$ mice in all three turns of the cochlea (afferent), and in the middle and basal turns of the cochlea (efferent). CtBP2 counts between WT and Spnb5$^{(-/-)}$ mice are not significantly different ($P>0.05$).

329

330

331 **DISCUSSION**

332 In this paper, we elucidate the function of βV spectrin in hearing using a mouse
333 gene deletion model. Removal of exon 2 containing the initiator methionine and an
334 N-terminal 37 amino acids, which, in part, compose its actin-binding domain,
335 results in a mouse with normal ABR thresholds, and normal measures of OHC
336 function including DPOAEs and NLC. Typical DPOAEs are a strong indication of
337 normal OHC electromotility (Shera & Guinan, 1999). The presence of normal NLC
338 measures further reiterates this interpretation. Moreover, we were unable to detect
339 Spnb5 mRNA in the organ of Corti or OHCs.

340

341 In contrast, we find a reduction in ABR wave I amplitudes that are concordant with
342 our finding of reduced numbers of nerve fibers. These data point to βV spectrin as
343 critical for the maintenance and function of afferent and efferent nerve fibers. The
344 normal ABR thresholds in the presence of reduced wave I amplitudes we observe

345 in mice have been seen previously in mutations of other proteins and, in particular,
346 in the recovery phase of noise-induced hearing loss (Maison, Pyott, Meredith, &
347 Liberman, 2013) (Kujawa & Liberman, 2009).
348
349 How do we explain the preserved ABR thresholds in the presence of reduced wave
350 I amplitudes? Loss of neurons of up to 80% has been shown to be associated with
351 normal thresholds as long as hair cells were functional (Schuknecht & Woellner,
352 1953). Although speculative, other authors have reasoned that a small increase in
353 sound pressure of 5 dB results in wider recruitment of neurons adjacent to the
354 index sound frequency that could compensate for a 50% loss in afferent neurons
355 using insensitive measures such as compound action potentials and ABRs
356 (Taberner and Liberman 2005), (Lin, Furman, Kujawa, & Liberman, 2011). An
357 important distinction in our data is that, unlike in noise-induced hearing loss
358 models, we see no differences in CtBP2 counts (Liberman & Kujawa, 2017). Our
359 CtBP2 counts and preliminary analysis using nerve counts suggest that the
360 functional effects in these mice lie in the nerve. Ongoing work in our lab includes
361 detailed analysis of high and low threshold fiber counts in these animals, together
362 with studies that will better determine the exact molecular mechanisms which
363 underlie the reduction in dendritic and axonal numbers.
364
365 We find absent effects on OHC function in Spnb5$^{(-/-)}$ mice that is consistent with
366 the undetectable expression of these transcripts in the cochlea and OHC in
367 particular. We note similar low/absent Spnb5 RNA expression upon interrogation

368 of both OHC single-cell RNA and OHC RNA expression datasets of adult mice that
369 have been published (Li et al., 2018) and gEAR portal (Shen, Scheffer, Kwan, &
370 Corey, 2015), (Liu, Chen et al. 2018), (Hoa et al., 2020). Together, these data
371 question the validity of βV spectrin antibody staining of OHCs, the principal reason
372 for ascribing its presence in OHCs (Legendre et al., 2008), (Cortese et al., 2017).
373 These papers led to the belief that βV spectrin had an integral role in the
374 cytoskeleton of hair cells. Our assertion that βV spectrin is not important for OHC
375 function is based, in part, on the absent phenotype in the knockout mice. It is
376 reasonable to ask if the knockout mouse resulted in an actual loss of function in
377 the gene. We feel confident that the deletion of the second exon in Spnb5$^{(-/-)}$
378 resulted in a silencing of the gene. In addition to the neuronal phenotype we
379 describe herein with the Spnb5$^{(-/-)}$ mice, we were also unable to detect Spnb5
380 transcript from the testis of knockout mice that may relate to degradation of
381 nonsense transcripts and a phenomenon observed in deletion of other genes
382 (Baker & Parker, 2004). RNAscope *in situ* hyridization data also show reduction in
383 the amount of detected mRNA in the SGN of KO animals. While the phenotype of
384 mice is consistent with the absent expression of Spnb5 transcript in OHCs, we
385 have to be mindful that normal OHC function in these mice could be due to other
386 beta spectrins substituting for Spnb5 spectrin. In this context, the presence of a
387 clear auditory phenotype in the Spnb2 spectrin knockout mice would suggest that
388 such an interchange and substitution by other spectrins is, however, not likely.
389 Moreover, Spnb4$^{(qv/qv)}$ spectrin has a neuronal phenotype, similar to Spnb5$^{(-/-)}$.
390

391 In conclusion, we present data in this study that βV spectrin plays an important role
392 in auditory function. Our data confirm that βV spectrin is necessary to maintain the
393 integrity or function of afferent and efferent nerves of the peripheral auditory
394 system. Importantly, our data show no evidence that βV spectrin has a function in
395 OHCs, as has been previously suggested.

396 **MATERIALS AND METHODS**

397 **Mice.**

398 All procedures conducted with mice were approved by the Institutional Animal Care
399 and Use Committee at the Yale University School of Medicine. C57BL/6J mice
400 were housed under pathogen-free conditions and maintained as a breeding
401 colony. In our studies, C57BL/6J mice were engineered to harbor a gene knockout
402 of Spnb5 (βV spectrin). The floxed exon 2 of Spnb5 was excised with Cre-
403 recombinase from embryonic stem (ES) cells in culture before injecting them into
404 mouse blastocysts under the guidance of the Yale Gene Targeting Center. This
405 construct was designed to create a constitutive loss of βV spectrin. For genotyping
406 animals, tail snips were collected from mice at their weaning age. Genomic DNA
407 was prepared by an overnight 56˚C incubation in tail lysis buffer 50mM Tris pH 8.0,
408 50mM KCL, 2.5mM EDTA, 0.4% Igepal, 0.4% Tween 20 supplemented with
409 Proteinase K (400 μg/ml). gDNA was assayed by PCR using the following primer
410 set: Forward 5'-CTGTCCGCCAAAGAGCAGGGGCCATG-3' Reverse 5'-
411 GATGTGGGGTCAGCCCAGCATCTCC-3' and PCR amplimers were visualized
412 on a 2% agarose gel.

413

414 **OHC isolation.**

415 Prestin-YFP mice of 2-3 months of age were euthanized, the cochleae extracted,
416 and the organ of Corti dissected in ice cold 1x DPBS. OHCs were dissociated by
417 enzymatic digestion with pre-warmed 0.05% trypsin for 8 minutes at 37˚C followed
418 by gentle trituration in 10% FBS in DMEM with a 1 mL pipette tip. The cell

419 suspension was spun at 1500 g for 10 minutes. The cell pellet was resuspended
420 in DMEM supplemented with 10% FBS and then filtered through a 40-micron cell
421 strainer. The cells were FACS sorted, and YFP-positive OHCs were collected.
422
423 **mRNA detection.**
424 Total RNA from mouse testis and the whole brain was either obtained from Takara
425 or prepared from 100 mg of testis tissue from 3-month old WT and βV KO
426 C57BL/6J animals with Trizol reagent (Chomczynski & Mackey, 1995). cDNA was
427 prepared with Superscript IV reverse transcriptase (ThermoFisher Scientific,
428 Waltham, MA,) and quantified with a Nanodrop spectrophotometer. Standard
429 procedures followed reagent manufacturer's directions for first-strand synthesis.
430 The organ of Corti and OHCs (prepared as described above) were isolated and
431 proteolyzed with 1 unit of proteinase K. After inactivating at 95˚C for 5 minutes,
432 non-purified RNA was treated with Superscript IV to generate cDNA. Gene-specific
433 PCR primers bridging consecutive exons were designed to ensure the exclusion
434 of genomic DNA from amplification in **Table 1**.
435
436 **RNAscope *in situ* Hybridization.**
437 RNAscope *in situ* hybridization was performed on cochlear whole mount tissue
438 using RNAscope Multiplex Fluorescent v2 Assay (Advanced Cell Diagnostics
439 (ACD), Inc. Newark, CA, USA) according to the manufacturer's instructions
440 (Document # 323100-USM). RNAscope Probes and RNAscope Mulitplex
441 Fluorescent Reagent Kit v2 (Catalog # 323100) required for the assay were

442 purchased directly from ACD. Briefly, the cochlear apical turn of the organ of Corti
443 was dissected in 1x DPBS and fixed in 4% PFA. Cochlear tissue was pre-treated
444 with hydrogen peroxidase for 10 min at room temperature (RT), then with Protease
445 Plus for 15 min at 40°C in the HybEZ II Oven (ACD). Tissues were washed thrice
446 with distilled water for 5 min each at RT. The RNAscope Assay used the following
447 probes: target probe for Spnb5 (Catalog # 548431); positive control probe, Kcnma1
448 (Catalog #476251-C2); and negative control probe, DapB (Catalog #310043). For
449 SGNs the two probes used were Epha4 (Catalog #419081) and tyrosine
450 hydroxylase (Catalog #317612-C3). All probes were pre-warmed (10 min at 40°C),
451 brought to RT, then hybridized to the tissue with an 8 h incubation at 40°C. After
452 the tissue was stored in 5x saline sodium citrate (SCC) overnight at RT, hybridized
453 probe signal was amplified at 40°C with the consecutive addition of three
454 amplifiers: AMP1 (30 min), AMP2 (30 min), and AMP3 (15 min). HRP signal was
455 developed with a 15 min incubation in HRP-C1 at 40°C. For a single label
456 experiment, the TSA plus fluorophore CY3, diluted (1:50), (TSA Fluorescence Kit,
457 Catalog # NEL760001KT; PerkinElmer, Inc., MA, USA) was added for 30 min at
458 40°C, followed by a 15 min treatment with HRP blocker at 40°C. For double
459 fluorescent experiments, probes were developed using both HRP-C1 and HRP-C2
460 with alternating treatments of each fluorophore (fluorescein and CY3) and the HRP
461 blocker step. Between steps, tissue was washed twice with 1x Wash Buffer for 2
462 min each at RT. Finally, tissue was mounted with Prolong Gold antifade reagent
463 with DAPI (Thermo Fisher Scientific, OR, USA) on a glass bottom dish, and

464 fluorescent signal was visualized and imaged using a confocal microscope (Zeiss
465 Observer Z1).
466
467 **Auditory brainstem responses (ABR).**
468 ABR measurements were conducted in a manner similar to that described by Song
469 *et. al.* (El-Hassar et al., 2019). Briefly, animals were anesthetized with 480 mg/kg,
470 i.p., chloral hydrate, and all recordings were conducted in a sound-attenuating
471 chamber (Industrial Acoustics Corp., Bronx, NY). A customized TDT System 3
472 (Tucker-Davis Technologies Inc., Alachua, FL) was used for ABR recordings.
473 Subdermal needle electrodes (Rochester Electro-Medical, Lutz, FL) were
474 positioned at the vertex (active, noninverting), the right infra-auricular mastoid
475 region (reference, inverting), and the left neck region (ground). Differentially
476 recorded scalp potentials were bandpass filtered between 0.05 and 3 kHz over a
477 15 ms epoch. A total of 400 responses were averaged for each waveform for each
478 stimulus condition.
479
480 Symmetrically shaped tone bursts were 3 ms long (1 ms raised cosine on/off ramps
481 and 1 ms plateau). All acoustic stimuli were delivered free field via a speaker (EC1
482 Electrostatic Speaker, Tucker-Davis Technologies) positioned 10 cm from the
483 vertex. Stimulus levels were calibrated using a 0.5-inch condenser microphone
484 (model 4016, ACO Pacific, Belmont, CA) positioned at the approximate location of
485 the animal's head during recording sessions and are reported in decibels of sound
486 pressure level (SPL; referenced to 20 μPa). Stimuli of alternating polarity were

487 delivered at a rate of 21/s. Tone burst responses were collected in half-octave
488 steps ranging from 32 to 2.0 kHz. Stimuli were presented in 5 dB decrements of
489 sound intensity from a maximum level of 90 dB SPL. The ABR threshold was
490 defined as the lowest intensity of sound level capable of evoking a reproducible,
491 visually detectable response. Latencies and amplitudes of the initial ABR wave
492 were determined at a frequency of 16 kHz, one of the most sensitive frequency of
493 hearing in mice. Latencies and amplitudes of wave I at 90 dB SPL were also
494 measured at all the other frequencies. The analysis was performed in BioSigRP,
495 a digital signal processing software (TDT), on traces with discernible peaks by
496 setting cursors at the maxima and minima of the peaks. Latency was defined as
497 the time from the onset of the stimulus to the peak, while amplitude was measured
498 by taking the mean of the ΔV of the positive and negative deflections of the ABR
499 wave.
500
501 **Distortion product otoacoustic emissions (DPOAEs).**
502 The acoustic stimuli for DPOAEs were produced, and responses were recorded
503 using a customized TDT System 3 (Tucker-Davis Technologies Inc., Alachua, FL)
504 controlled by BioSigRP (TDT). To deliver acoustic stimuli and record the
505 responses, two speakers (MF1 Multi-Field Magnetic Speakers, TDT) and a
506 microphone probe (ER-10B+, Etymotic Research, Elk Grove Village, IL) were
507 connected by short PVC tubing, and the microphone probe was inserted into the
508 external auditory meatus of the anaesthetized mouse via a tapered plastic pipette
509 tip. Two simultaneous continuous pure tones (f_1 and f_2) that have a frequency ratio

510 of 1.2 (f_2/f_1) and equal sound level ($L_1 = L_2$) were delivered at center frequencies
511 of 8, 12, 16, 24 and 32 kHz with sound levels from 80 to 20 dB SPL in 10 dB
512 decrements. Stimuli duration was 83.88 ms at a repetition rate of 11.92 per second.
513 The acquired DPOAE responses were averaged 100 times. The DPOAE of interest
514 was at $2f_1$-f_2, the largest and most prominent DPOAE. The DPOAE threshold was
515 defined as the lowest sound intensity capable of evoking a visually detectable $2f_1$-
516 f_2 signal above the noise floor. DPOAE amplitudes were analyzed offline in
517 BioSigRP by setting cursors at the peak of the $2f_1$-f_2 signals.
518
519 **Nonlinear capacitance (NLC).**
520 Nonlinear capacitance was conducted in a fashion much like that previously
521 described (Song & Santos-Sacchi, 2016). C57BL/6J WT and βV spectrin KO
522 littermates at postnatal day 13 and at 2 months of age were compared. Apical turns
523 of the organ of Corti were isolated from each and recorded with ionic current
524 blocking solutions to minimize interference on measures of membrane
525 capacitance. The extracellular solution contained (in mM): 100 NaCl, 20
526 tetraethylammonium (TEA)-Cl, 20 CsCl, 2 $CoCl_2$, 1 $MgCl_2$, 1 $CaCl_2$, 10 HEPES,
527 pH 7.2. The intracellular solution contained (in mM): 140 CsCl, 2 $MgCl_2$, 10
528 HEPES, and 10 EGTA, pH 7.2. Pipettes had resistances of 3-5 MΩ. Gigohm seals
529 were made, and stray capacitance was balanced out with amplifier circuitry prior
530 to establishing whole-cell conditions. A Nikon Eclipse E600-FN microscope with
531 40× water immersion objective lens was used to observe cells during voltage
532 clamp. Whole-cell voltage-clamp recordings were performed from all three rows of

533 OHCs on whole-mount organ of Corti. OHCs were recorded at room temperature
534 using jClamp software and an Axopatch 200B amplifier (Molecular Devices, LCC,
535 San Jose, CA). Data were low pass filtered at 10 kHz and digitized at 100 kHz with
536 a Digidata 1320A (Molecular Devices, LCC, San Jose, CA). In order to extract
537 Boltzmann parameters, capacitance-voltage data were fit to the first derivative of
538 a two-state Boltzmann function.

539

540
541 $$C_m = NLC + C_{sa} + C_{\text{lin}} = Q_{\text{max}} \frac{\text{ze}}{k_B T} \frac{b}{(1+b)^2} + C_{sa} + C_{\text{lin}} \quad \text{(eq.1)}$$
542
543
544 where $b = exp\left(-ze\frac{V_m - V_h}{k_B T}\right)$, $C_{sa} = \frac{\Delta C_{sa}}{(1+b^{-1})}$
545
546 Q_{max} is the maximum nonlinear charge moved, V_h is the voltage at peak
547 capacitance or equivalently, at half-maximum charge transfer, V_m is R_s-corrected
548 membrane potential, z is valence, C_{lin} is linear membrane capacitance, e is the
549 electron charge, kB is Boltzmann's constant, and T is the absolute temperature.

550

551 **Immunohistochemistry.**

552 For immunohistochemistry, staining was performed on fixed and decalcified three
553 turns of the organ of Corti to compare the number of neuronal fibers and synapses
554 between all three cochlear turns in KO and WT mice. Temporal bones were fixed
555 in 4% PFA overnight at 4˚C and then decalcified in 120 mM
556 ethylenediaminetetraacetic acid (EDTA) for 2 days. Whole-mount of the organ of
557 Corti was dissected, washed in PBS 0.05% Tween 20, 0.05% Triton-X 100
558 (incubation buffer) three times for 3 minutes each, and incubated with primary

559 antibody in incubation buffer overnight at 4˚C with mouse anti-CtBP2 antibody
560 (1:50, BD Transduction, San Jose, CA, cat# 612044), chicken anti-neurofilament
561 (NF) antibody (1:500, MilliporeSigma, Billerica, MA, cat# AB5539). After three
562 washes in incubation buffer, the tissue was incubated with secondary antibody in
563 incubation buffer for 1 hour at room temperature. The secondary antibodies used
564 included donkey anti-rabbit Alexa Fluor 568/647 (1:200; Thermo Fisher Scientific,
565 cat # A-10042/A-31573), goat anti-mouse Alexa Fluor 568/647 (1:200; Thermo
566 Fisher Scientific, cat # A-21124/A-21235) and goat anti-chicken Alexa Fluor
567 488/594 (1:200; Thermo Fisher Scientific, cat # A-11039/A-11042). After antibody
568 treatment, cells were washed in incubation buffer and mounted in Vectashield
569 (Vector Laboratories, Inc., Burlingame, CA), and viewed using a Zeiss confocal
570 laser-scanning microscope (Oberkochen, Germany).
571
572 Nerve (NF positive) and synaptic vesicle (CtBP2 positive) counts were performed
573 posthoc in Fiji (ImageJ). Briefly, z stacks of images were separated by probes,
574 background-subtracted (using a 50-pixel rolling ball radius), and z sections
575 containing the images of interest identified for further analysis (slice keeper).
576 CtBP2 labeled IHCs and NF labeled afferent fibers surrounding IHCs in proximity
577 to the habenula and efferent fibers in the cochlear canal were counted. Z
578 projections (sum) of the respective sections were obtained and automated
579 thresholds determined (max entropy). Counts of particles (synaptic vesicles)
580 immunopositive for CtBP2 larger than 0.1 microns were scored. Neuronal numbers
581 were established by counting the peaks in a profile plotted perpendicular to neural

582 fibers in the cochlea canal. For afferent nerve counts the profile was plotted at the
583 midpoint of nerve densities.
584
585 **Statistical Analysis**.
586 Data were analyzed using FIJI, Microsoft Excel, SigmaPlot and GraphPad Prism.
587 The measures of variability are depicted as error bars +/- the SEM and stated
588 numerically in the figure legends. Unpaired, one or two-tailed Student's t-test were
589 performed using both Excel and GraphPad Prism to make comparisons between
590 WT and Spnb5$^{(-/-)}$ data points. P-values are indicated in the figure legends to two
591 significant figures. The sample size (n) is stated in the figures.
592
593 **COMPETING INTERESTS**
594 The authors declare no competing interests.
595
596 **AUTHOR CONTRIBUTIONS**
597 MCS, JPB, JSM, DN and JSS conceptualized the project. PRS and JSM
598 generated the Spnb5 deleted mice. MCS and JPB conducted animal breeding,
599 tissue collection and genotyping. MCS, JPB, SK, WT, AS and DN performed gene
600 expression and immunohistochemistry analysis. JPB and LS performed assays to
601 assess hearing function. MCS and DN wrote the manuscript, and all authors
602 contributed to its editing and refinement.
603
604 **ACKNOWLEDGEMENTS**

605 These studies were supported by grants R01 DC 008130 and R01 DC 008130
606 from the National Institute of Health to JSS and DN and grants P01 NS35476
607 (project 4) and R01 HL28560 to JSM. Other support includes the Raymond Yesner
608 Endowment to Yale University (JSM). We also would like to thank Lan Ji for her
609 technical assistance.
610

611 **REFERENCES**
612

613 Abe, T., Kakehata, S., Kitani, R., Maruya, S., Navaratnam, D., Santos-Sacchi, J.,
614 & Shinkawa, H. (2007). Developmental expression of the outer hair cell
615 motor prestin in the mouse. *J Membr Biol, 215*(1), 49-56.
616 doi:10.1007/s00232-007-9004-5

617 Bai, J. P., Surguchev, A., Ogando, Y., Song, L., Bian, S., Santos-Sacchi, J., &
618 Navaratnam, D. (2010). Prestin surface expression and activity are
619 augmented by interaction with MAP1S, a microtubule-associated protein.
620 *J Biol Chem, 285*(27), 20834-20843. doi:10.1074/jbc.M110.117853

621 Baker, K. E., & Parker, R. (2004). Nonsense-mediated mRNA decay: terminating
622 erroneous gene expression. *Curr Opin Cell Biol, 16*(3), 293-299.
623 doi:10.1016/j.ceb.2004.03.003

624 Benson, D. A., Cavanaugh, M., Clark, K., Karsch-Mizrachi, I., Lipman, D. J.,
625 Ostell, J., & Sayers, E. W. (2013). GenBank. *Nucleic Acids Res,*
626 *41*(Database issue), D36-42. doi:10.1093/nar/gks1195

627 Bramhall, N. F., McMillan, G. P., Kujawa, S. G., & Konrad-Martin, D. (2018). Use
628 of non-invasive measures to predict cochlear synapse counts. *Hear Res,*
629 *370*, 113-119. doi:10.1016/j.heares.2018.10.006

630 Chomczynski, P., & Mackey, K. (1995). Short technical reports. Modification of
631 the TRI reagent procedure for isolation of RNA from polysaccharide- and
632 proteoglycan-rich sources. *Biotechniques, 19*(6), 942-945. Retrieved from
633 https://www.ncbi.nlm.nih.gov/pubmed/8747660

634 Consortium, G. T. (2013). The Genotype-Tissue Expression (GTEx) project. *Nat*
635 *Genet, 45*(6), 580-585. doi:10.1038/ng.2653

636 Cortese, M., Papal, S., Pisciottano, F., Elgoyhen, A. B., Hardelin, J. P., Petit, C., .
637 . . El-Amraoui, A. (2017). Spectrin betaV adaptive mutations and changes
638 in subcellular location correlate with emergence of hair cell electromotility
639 in mammalians. *Proc Natl Acad Sci U S A, 114*(8), 2054-2059.
640 doi:10.1073/pnas.1618778114

641 Cousin, M., Breau, K., Creighton, B.A., Spillmann, R.C., Torti, E., Dontu, S.,
642 Tripathi, S., Ajit, D., Harper, K.M., Stankewich, M.C… Lorenzo, D.N.
643 (2020). Pathogenic SPTBN1 variants cause a novel autosomal dominant

644 neurodevelopmental syndrome. medRxiv 2020.08.31.20184481; doi:
645 https://doi.org/10.1101/2020.08.31.20184481
646

647 Efimova, N., Korobova, F., Stankewich, M. C., Moberly, A. H., Stolz, D. B., Wang,
648 J., . . . Svitkina, T. (2017). betaIII Spectrin Is Necessary for Formation of
649 the Constricted Neck of Dendritic Spines and Regulation of Synaptic
650 Activity in Neurons. *J Neurosci, 37*(27), 6442-6459.
651 doi:10.1523/JNEUROSCI.3520-16.2017

652 El-Hassar, L., Song, L., Tan, W. J. T., Large, C. H., Alvaro, G., Santos-Sacchi, J.,
653 & Kaczmarek, L. K. (2019). Modulators of Kv3 Potassium Channels
654 Rescue the Auditory Function of Fragile X Mice. *J Neurosci, 39*(24), 4797-
655 4813. doi:10.1523/JNEUROSCI.0839-18.2019

656 Hafidi, A., Despres, G., & Romand, R. (1990). Cochlear innervation in the
657 developing rat: an immunocytochemical study of neurofilament and
658 spectrin proteins. *J Comp Neurol, 300*(2), 153-161.
659 doi:10.1002/cne.903000202

660 Hammarlund, M., Jorgensen, E. M., & Bastiani, M. J. (2007). Axons break in
661 animals lacking beta-spectrin. *J Cell Biol, 176*(3), 269-275.
662 doi:10.1083/jcb.200611117

663 Hoa, M., Olszewski, R., Li, X., Taukulis, I., Gu, S., DeTorres, A., . . . Kelley, M.
664 W. (2020). Characterizing Adult Cochlear Supporting Cell Transcriptional
665 Diversity Using Single-Cell RNA-Seq: Validation in the Adult Mouse and
666 Translational Implications for the Adult Human Cochlea. *Front Mol*
667 *Neurosci, 13*, 13. doi:10.3389/fnmol.2020.00013

668 Holley, M. C., & Ashmore, J. F. (1990). Spectrin, actin and the structure of the
669 cortical lattice in mammalian cochlear outer hair cells. *J Cell Sci, 96 (Pt*
670 *2)*, 283-291. Retrieved from http://www.ncbi.nlm.nih.gov/pubmed/2211870

671 Holley, M. C., Kalinec, F., & Kachar, B. (1992). Structure of the cortical
672 cytoskeleton in mammalian outer hair cells. *J Cell Sci, 102 (Pt 3)*, 569-
673 580. Retrieved from https://www.ncbi.nlm.nih.gov/pubmed/1506434

674 Kujawa, S. G., & Liberman, M. C. (2009). Adding insult to injury: cochlear nerve
675 degeneration after "temporary" noise-induced hearing loss. *J Neurosci,*
676 *29*(45), 14077-14085. doi:10.1523/JNEUROSCI.2845-09.2009

677 Legendre, K., Safieddine, S., Kussel-Andermann, P., Petit, C., & El-Amraoui, A.
678 (2008). alphaII-betaV spectrin bridges the plasma membrane and cortical
679 lattice in the lateral wall of the auditory outer hair cells. *J Cell Sci, 121*(Pt
680 20), 3347-3356. doi:10.1242/jcs.028134

681 Lewis, M. A., Nolan, L. S., Cadge, B. A., Matthews, L. J., Schulte, B. A., Dubno,
682 J. R., . . . Dawson, S. J. (2018). Whole exome sequencing in adult-onset
683 hearing loss reveals a high load of predicted pathogenic variants in known
684 deafness-associated genes and identifies new candidate genes. *BMC*
685 *Med Genomics, 11*(1), 77. doi:10.1186/s12920-018-0395-1

686 Li, Y., Liu, H., Giffen, K. P., Chen, L., Beisel, K. W., & He, D. Z. Z. (2018).
687 Transcriptomes of cochlear inner and outer hair cells from adult mice. *Sci*
688 *Data, 5*, 180199. doi:10.1038/sdata.2018.199

689 Liberman, M. C., & Kujawa, S. G. (2017). Cochlear synaptopathy in acquired
690 sensorineural hearing loss: Manifestations and mechanisms. *Hear Res,*
691 *349*, 138-147. doi:10.1016/j.heares.2017.01.003

692 Lin, H. W., Furman, A. C., Kujawa, S. G., & Liberman, M. C. (2011). Primary
693 neural degeneration in the Guinea pig cochlea after reversible noise-
694 induced threshold shift. *J Assoc Res Otolaryngol, 12*(5), 605-616.
695 doi:10.1007/s10162-011-0277-0

696 Liu, Y., Qi, J., Chen, X., Tang, M., Chu, C., Zhu, W., . . . Zhong, G. (2019).
697 Critical role of spectrin in hearing development and deafness. *Sci Adv,*
698 *5*(4), eaav7803. doi:10.1126/sciadv.aav7803

699 Lorenzo, D. N., Badea, A., Zhou, R., Mohler, P. J., Zhuang, X., & Bennett, V.
700 (2019). betaII-spectrin promotes mouse brain connectivity through
701 stabilizing axonal plasma membranes and enabling axonal organelle
702 transport. *Proc Natl Acad Sci U S A, 116*(31), 15686-15695.
703 doi:10.1073/pnas.1820649116

704 Maison, S. F., Pyott, S. J., Meredith, A. L., & Liberman, M. C. (2013).
705 Olivocochlear suppression of outer hair cells in vivo: evidence for
706 combined action of BK and SK2 channels throughout the cochlea. *J*
707 *Neurophysiol, 109*(6), 1525-1534. doi:10.1152/jn.00924.2012

708 Melcher, J. R., Knudson, I. M., Fullerton, B. C., Guinan, J. J., Jr., Norris, B. E., &
709 Kiang, N. Y. (1996). Generators of the brainstem auditory evoked potential

in cat. I. An experimental approach to their identification. *Hear Res, 93*(1-2), 1-27. doi:10.1016/0378-5955(95)00178-6

Papal, S., Cortese, M., Legendre, K., Sorusch, N., Dragavon, J., Sahly, I., . . . El-Amraoui, A. (2013). The giant spectrin betaV couples the molecular motors to phototransduction and Usher syndrome type I proteins along their trafficking route. *Hum Mol Genet, 22*(18), 3773-3788. doi:10.1093/hmg/ddt228

Parkinson, N. J., Olsson, C. L., Hallows, J. L., McKee-Johnson, J., Keogh, B. P., Noben-Trauth, K., . . . Tempel, B. L. (2001). Mutant beta-spectrin 4 causes auditory and motor neuropathies in quivering mice. *Nat Genet, 29*(1), 61-65. doi:10.1038/ng710

Schuknecht, H. F., & Woellner, R. C. (1953). Hearing losses following partial section of the cochlear nerve. *Trans Am Laryngol Rhinol Otol Soc, 58*(57th Meeting), 369-393; discussion, 393-364. Retrieved from https://www.ncbi.nlm.nih.gov/pubmed/13146770

Sergeyenko, Y., Lall, K., Liberman, M. C., & Kujawa, S. G. (2013). Age-related cochlear synaptopathy: an early-onset contributor to auditory functional decline. *J Neurosci, 33*(34), 13686-13694. doi:10.1523/JNEUROSCI.1783-13.2013

Shen, J., Scheffer, D. I., Kwan, K. Y., & Corey, D. P. (2015). SHIELD: an integrative gene expression database for inner ear research. *Database (Oxford), 2015*, bav071. doi:10.1093/database/bav071

Shera, C. A., & Guinan, J. J., Jr. (1999). Evoked otoacoustic emissions arise by two fundamentally different mechanisms: a taxonomy for mammalian OAEs. *J Acoust Soc Am, 105*(2 Pt 1), 782-798. doi:10.1121/1.426948

Song, L., McGee, J., & Walsh, E. J. (2006). Frequency- and level-dependent changes in auditory brainstem responses (ABRS) in developing mice. *J Acoust Soc Am, 119*(4), 2242-2257. doi:10.1121/1.2180533

Song, L., & Santos-Sacchi, J. (2016). A Walkthrough of Nonlinear Capacitance Measurement of Outer Hair Cells. *Methods Mol Biol, 1427*, 501-512. doi:10.1007/978-1-4939-3615-1_28

741 Stabach, P. R., & Morrow, J. S. (2000). Identification and characterization of beta
742 V spectrin, a mammalian ortholog of Drosophila beta H spectrin. *J Biol*
743 *Chem, 275*(28), 21385-21395. doi:10.1074/jbc.C000159200

744 Stankewich, M. C., Cianci, C. D., Stabach, P. R., Ji, L., Nath, A., & Morrow, J. S.
745 (2011). Cell organization, growth, and neural and cardiac development
746 require alphaII-spectrin. *J Cell Sci, 124*(Pt 23), 3956-3966.
747 doi:10.1242/jcs.080374

748 Stankewich, M. C., Gwynn, B., Ardito, T., Ji, L., Kim, J., Robledo, R. F., . . .
749 Morrow, J. S. (2010). Targeted deletion of betaIII spectrin impairs
750 synaptogenesis and generates ataxic and seizure phenotypes. *Proc Natl*
751 *Acad Sci U S A, 107*(13), 6022-6027. doi:10.1073/pnas.1001522107

752 Yue, F., Cheng, Y., Breschi, A., Vierstra, J., Wu, W., Ryba, T., . . . Mouse, E. C.
753 (2014). A comparative encyclopedia of DNA elements in the mouse
754 genome. *Nature, 515*(7527), 355-364. doi:10.1038/nature13992
755
756

757
758 **Table1. Beta spectrin gene specific primers.**

Primers					Amplimer (bps)
Spnb1	forward	CAAAGAGCAGGAGGTGTCAGC	reverse	TCTAGGCAGGTGCTGAAGTTC	264
	nested forward	GATGCGTGTGCCGGGCGCC	nested reverse	CTGGTATTGATCTCTGCCT	197
Spnb2	forward	CCGGTGGGAGTGGTTAAGAC	reverse	CATCCCAGGTCGCTGCAGAC	188
	nested forward	GATTTTGGAGGTCCATCAG	nested reverse	TCAAACGCCTCATGGCGCT	144
Spnb5	forward	CTCCGGAGCTTTGAGCAGGCTGC	reverse	CCTGAGCCCACGCTAGCAATTCC	439
	nested forward	GATACAGGAGAAGACCACC	nested reverse	TTCCTGGACTTTGGCCTCC	319
Spnb5	forward	TGGCCTTCCTCAGGGCCAAGGT	reverse	GCACTCATCTGGATGCAGGGCTG	440
	nested forward	CTTGGACAGGGAGGAGTTTGG	nested reverse	GCACTCATCTGGATGCAGGGCTG	313

759
760 Primer sets were used to detect for mRNA of Spnb1, Spnb2, and Spnb5 in the
761 brain, organ of Corti, and isolated OHCs. The PCR amplimer sizes from mRNA
762 are presented in the final column.
763
764 **Table 2. Primers for the Spnb5 gene used to prepare the three DNA fragments**
765 **that were subcloned into pEasy-Flox.**

Fragment 1	forward	CAGCGGCCGCAGGGGCTGCCTCCTACTGTACC	reverse	GAGCGGCCGCACTTGAATGACCCAGAGCCACCCCT
Fragment 2	forward	GGTCTAGACCTCTTACTCGCTTAGGTTCCAATC	reverse	GCTCTAGATGACTCTACAGCAGACCCCCAGGTC
Fragment 3	forward	GACTCGAGCCTGTAGCTATTTCTGGCCTACCCCTCC	reverse	GACTCGAGGGAGGGAGGGTTACTGTAGTAGAAGGGC

766
767 The targeting vector for homologous recombination was constructed by cloning
768 three PCR generated fragments into the pEASY-Flox vector. Fragment 1 is a 4115
769 bp product, fragment 2 is a 469 bp product that contains Spnb5 exon 2, and
770 fragment 3 is 4371 bp of sequence that spans up to exon 5. The three fragments
771 were sequence verified. The oligos contain common restriction sites at their 5' end
772 for easy cloning into the targeting vector.
773
774 **Table 3. Primers for rt-PCR in WT and Spnb5$^{(-/-)}$ tissue.**

Spnb5	exon 58/60	forward	CTCCGGAGCTTTGAGCAGGCTGC	reverse	CCTGAGCCCACGCTAGCAATTCC	439
Spnb5	exon 53/55	forward	AGGAGAAACACCAGAATTTGGAGAATG	reverse	TGTCCACTCTCCAGAAGGGCAACTG	412
Spnb2	exon 28/29	forward	GATACAGGAGAAGACCACC	reverse	TTCCTGGACTTTGGCCTCC	144
Spna2	exon 54/55	forward	AACAGGAGTGACTGAGGAGG	reverse	CCTTCCTCAACCATTGGCAGA	144

775
776 These primer sets were tested on cDNA from testis isolated from WT and Spnb5$^{(-}$
777 $^{/-)}$ 3-month-old mice. Because the C-terminus of these large genes tends to be
778 more abundant than N-terminus exons, we designed primer sets that will amplify
779 exons near the poly-A tail.
780
781